Situation-Based Neuromorphic Memory in Spiking Neuron-Astrocyte Network

Susanna Gordleeva, Yuliya A. Tsybina, Mikhail I. Krivonosov, Ivan Y. Tyukin, Victor B. Kazantsev, Alexey Zaikin, and Alexander N. Gorban

***Abstract*— Mammalian brains operate in very special surroundings: to survive they have to react quickly and effectively to the pool of stimuli patterns previously recognized as danger. Many learning tasks often encountered by living organisms involve a specific set-up centered around a relatively small set of patterns presented in a particular environment. For example, at a party, people recognize friends immediately, without deep analysis, just by seeing a fragment of their clothes. This set-up with reduced "ontology" is referred to as a "situation." Situations are usually local in space and time. In this work, we propose that neuron-astrocyte networks provide a network topology that is effectively adapted to accommodate situation-based memory. In order to illustrate this, we numerically simulate and analyze a well-established model of a neuron-astrocyte network, which is subjected to stimuli conforming to the situation-driven environment. Three pools of stimuli patterns are considered: external patterns, patterns from the situation associative pool regularly presented to the network and learned by the network, and patterns already learned and remembered by astrocytes. Patterns from the external world are added to and removed from the associative pool. Then, we show that astrocytes are structurally necessary for an effective function in such a learning and testing set-up. To demonstrate this we present a novel neuromorphic computational model for short-term memory implemented by a two-net spiking neural-astrocytic network. Our results show that such a system tested on synthesized data with selective astrocyte-induced modulation of neuronal activity provides an enhancement of retrieval quality in comparison to standard spiking neural networks trained via Hebbian plasticity only. We argue that the proposed set-up may offer a new way to analyze, model, and understand neuromorphic artificial intelligence systems.**

***Index Terms*— Astrocyte, neuromorphic computing, neuron-astrocyte interaction, spiking neural network, working memory.**

Manuscript received 14 March 2022; revised 4 April 2023 and 19 August 2023; accepted 13 November 2023. The work of Ivan Y. Tyukin and Alexander N. Gorban was supported by the UK Research and Innovation (UKRI) Turing AI Fellowship EP/V025295/2. *(Corresponding author: Susanna Gordleeva.)*

Susanna Gordleeva and Victor B. Kazantsev are with the Department of Neurotechnologies, Lobachevsky State University of Nizhny Novgorod, 603950 Nizhny Novgorod, Russia, and also with the Laboratory of Neurobiomorphic Technologies, Moscow Institute of Physics and Technology, 141701 Moscow, Russia (e-mail: gordleeva@neuro.nnov.ru; kazantsev@neuro.nnov.ru).

Yuliya A. Tsybina is with the Department of Neurotechnologies, Lobachevsky State University of Nizhny Novgorod, 603950 Nizhny Novgorod, Russia, and also with the Centre for Analysis of Complex Systems, Sechenov First State Medical University, 119435 Moscow, Russia (e-mail: lotarevaj@gmail.com).

Mikhail I. Krivonosov is with the Department of Neurotechnologies, Lobachevsky State University of Nizhny Novgorod, 603950 Nizhny Novgorod, Russia (e-mail: mike_live@mail.ru).

Ivan Y. Tyukin is with the Department of Mathematics, King's College London, WC2R 2LS London, U.K. (e-mail: ivan.tyukin@kcl.ac.uk).

Alexey Zaikin is with the Institute for Women's Health and Department of Mathematics, University College London, WC1H 0AY London, U.K., also with the Department of Neurotechnologies, Lobachevsky State University of Nizhny Novgorod, 603950 Nizhny Novgorod, Russia, also with the Centre for Analysis of Complex Systems, Sechenov First State Medical University, 119435 Moscow, Russia, also with the Institute for Cognitive Neuroscience, University Higher School of Economics, 119991 Moscow, Russia, and also with the Britton Chance Center for Biomedical Photonics, Wuhan National Laboratory for Optoelectronics, Huazhong University of Science and Technology, Wuhan 430074, China (e-mail: alexey.zaikin@ucl.ac.uk).

Alexander N. Gorban is with the Department of Mathematics, King's College London, WC2R 2LS London, U.K., and also with the School of Computing and Mathematical Sciences, University of Leicester, LE1 7RH Leicester, U.K. (e-mail: a.n.gorban@leicester.ac.uk).

This article has supplementary material provided by the authors and color versions of one or more figures available at https://doi.org/10.1109/TNNLS.2023.3335450.

Digital Object Identifier 10.1109/TNNLS.2023.3335450

I. Introduction

THE way the test data is organized, and validated, as well as the method used to train learning systems can critically affect the result. Especially, if the quality of learning is directly linked to survival. Mammalian brains are trained to survive, which is why they enable an animal to react quickly to patterns previously associated with dangerous situations. Hence, it is important to understand how such quick responses emerge in highly uncertain and complicated real-world operational conditions.

The cornerstone assumption of the classical statistical learning frameworks [1], [2], [3] is that a learner or a learning machine operates in an environment that can be adequately modeled by some unknown probability distribution. The learner then gathers relevant information about the environment by accessing independent samples from this unknown distribution. The problem, however, is that these apparently sensible classical assumptions have major consequences affecting the applicability of the theory. The independence assumption may be violated when the learner's training data inherits strong temporal correlations (e.g., subsequent frames taken from video footage) and which have been ignored at the data-processing stage. The absence of any knowledge about the fixed probability distribution, which is particularly difficult to alleviate in high-dimensional settings, enforces conservative worst case distribution-agnostic generalization bounds [1], [2], [3] and can lead to a stream of foundational paradoxes highlighting the potential impossibility to compute stable and accurate learning machines [4].[1] Finally,

[1]See also Theorem 7.1 from [1] showing that an arbitrarily small perturbation added to an activation function has the capacity to make the Vapnik-Chervonenkis dimension of a neuron with this modified activation function infinite and hence rendering all classical generalization bounds using Vapnik-Chervonenkis dimension useless for neural networks with such neurons.

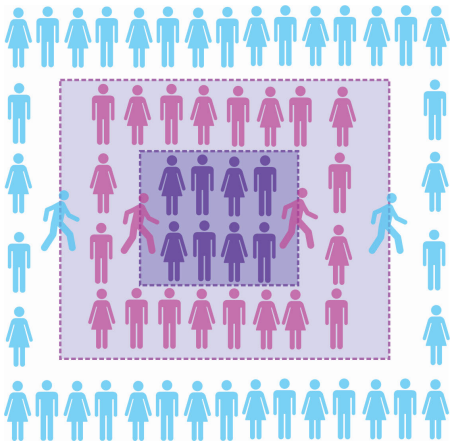

Fig. 1. Diagram of a situation-based model of data. In this model, all data are partitioned into three pools of patterns. The largest circle of patterns (light blue) is the external world that contains a huge number of patterns. A situation-based pool of patterns is much smaller and includes only the patterns that we meet regularly within this situation (purple). Data patterns in the situation-based pool can be removed and replaced with patterns from the external world. Patterns from this pool are used for learning much more often than a random pattern from the external world pool, hence many of them are already learned, stored, and can be easily and quickly recognized by association with patterns stored in the system (dark blue lila).

the fact that the distribution is fixed and unknown has an impact on the possibility of handling concept drifts—a widespread phenomenon in real-life practical applications [5]. We suggest that the above difficulties can potentially be overcome via the introduction of a new mode of learning which we will refer to as *situation-based learning*.

How many people did you meet yesterday? 5? or 10? Was it difficult to recognize them? Psychologists say that our day-to-day activities impact our behavior. Recognition of patterns around us occurs in, what is called in psychology, a situation. Obviously, biological creatures that require less time to recognize a situation are getting an evolutionary advantage, they can escape a predator faster, get a higher chance of catching prey, or when humans are concerned, earn more money. We all live in a situation-ridden world, and our life is based on the recognition of patterns in the current situation. But how is this recognition organized? We do not normally spend much time recognizing a friend, a fraction of a pattern is usually enough. Such quick processing is provided by a very special structure of pattern learning. We learn patterns from a situation-based pool, and, since the number of patterns in the situation is limited, our pool usually is much smaller than in the whole external world. Such a situation-based structure of learning is visualized in Fig. 1. There are three pools of patterns. Patterns from the huge external pool get into a situation-based pool, and then they become available for learning much more often than the ones arriving directly from the external pool. Hence, all patterns from a situation pool, except for the newcomers, are learned and stored in the memory—the internal pool. Recognition is, hence, structure-associated, and patterns from the structure pool are recognized much easier and quicker patterns than from an external pool.

Obviously, such a situation-based structure has two main advantages: it is quick and requires less energy, which is very important in the biological world. Creatures adapted to such structure-oriented patterns of learning are more competitive and have an evolutionary advantage. This new data model is complementary to other important characteristics of learning and memory explored in the previous work, including high-dimensionality of the space of stimuli [6], [7] and properties of data distributions conforming to the task of learning from few examples [8], [9]. The importance of the problem was mentioned by [10], [11]. The notion of the situation captures the spatiotemporal localization of the task and the subjectivity of learners, i.e., the relevant contexts. This enables a learner to partition the complexity of the environment into the union of much simpler "sparse" tasks. A related notion of *attention* in deep learning has already been proven successful in the area of natural language processing giving rise to the popular *transformer* models [12]. Here, we formalize the notion at the conceptual level regardless of its particular implementation in a learning machine.

All this leads to the key question of whether there exists a structural organization of neural circuitry that is particularly suited for structure-based learning and that possesses characteristics of information processing in these circuits that are necessary to support this learning. In this article, we propose relevant neural circuits that are particularly suited to facilitate situation-based learning. These circuits or networks combine conventional neurons and astrocytes.

The structural, metabolic, and homeostatic functions of astrocytes are well established [13]. Recently it has been revealed that astrocytes contribute to neural information processing via bidirectional exchange of regulatory signals with the neuronal elements. Astrocytes respond to neural activity by intracellular calcium elevations [14]. Calcium pulses in astrocytes induce the release of chemical transmitters (termed "gliotransmitters") which then regulate the synaptic gain of near and distant tripartite synapses at diverse timescales [15]. The data show that astrocytes have an impact on local synaptic plasticity, neuronal network oscillations, memory, and behavior (for recent reviews see [16], [17], [18]). Despite that the role played by astrocytes is not yet fully understood, these recent findings support the hypothesis that cognitive processing and memory are not the result of neuronal activity only but of the coordinated activity of both astrocytes and neurons [19]. Consequently, the most interesting research question is: whether the presence of astrocytes, which provide multiplex topology of a recognition network with different time and spatial scales of communication, facilitates the ability of the network to work with structure-associated learning? In this article, we investigate this question and show numerically that neuron-astrocyte networks indeed play a key role in situation-based recognition. This function is also closely linked to the idea of local corrections in large neural networks working with big data [7].

II. Related Work

Although astrocytic involvement in the information processing in the brain has been widely shown experimentally [16], there is a lack of computational studies of neural circuits focusing on astrocyte signaling in the context of learning and memory. The importance of computational modeling for developing a better understanding of nature and findings answers to open questions is difficult to overestimate. Examples of works where such modeling brought new

knowledge are numerous. In the area of astrocyte modeling, a recent study [20] successfully demonstrated the self-repairing capability of a distributed spiking neuron-astrocyte network (SNAN) in a robotic obstacle avoidance application. Nazari et al. [21] studied the information transmission between the cortical spiking neural network and the cortical neuron–astrocyte network. They showed how the cortical spiking network managed to improve its pattern recognition performance without the need for retraining by receiving additional information from a neuron-astrocyte network. In addition, scholars proposed several digital implementations of astrocytic dynamics [22] and neuron-astrocyte interaction [23], [24]. In our previous works, we investigated how the astrocyte-induced dynamic coordination in the neuronal ensembles [25], [26] induces the generation of integrated information sets [27], [28], [29]. Moreover, we showed that a biologically inspired SNAN can implement the multiitem short-term memory [30], [31]. We revealed that several information patterns can be maintained in memory at the time scale of calcium elevation in astrocytes, while the readout by the neurons due to the astrocyte-induced activity-dependent short-term synaptic plasticity resulted in local spatial synchronization in neuronal ensembles. Following our approach, a recent modeling study [32] investigated the contribution of astrocytic modulation of synaptic transmission to the formation of different modes of short-term working memory encoding. Another computational model predicts that the duration and stability of working memory representations can be altered by astrocytic signaling [33]. We further showed that the SNAN can reliably store not only binary but also analogous information patterns in short-term memory [34]. However, the work in this article goes much further and proposes a new bio-inspired two-net SNAN for more complex learning tasks, in which SNAN is implemented for associated learning.

III. Significance

In this article, we present three key findings: 1) a novel approach to formalizing machine learning data, namely, the temporal organization of the data as opposed to the widely accepted IID data sampling; 2) a novel neuromorphic computational model for short-term memory implemented by SNAN; and 3) a proof, through rigorous computational experiments, that SNAN tested on synthesized data with selective astrocyte-induced modulation of neuronal activity may provide an enhancement of retrieval quality in comparison to a standard SNN trained via Hebbian plasticity. The proposed SNAN is a hybrid system, which combines the fast-spiking neural networks pretrained by the spike-timing-dependent plasticity (STDP) rule with the general dataset, and a slow astrocytic network, which provides time-dependent data buffering via calcium activity and gliatransmitter-induced spatial-temporal coordination of neural network activity.

IV. Situation-Based Learning in SNAN Model

The concept of the proposed situation-based memory model is schematically summarized in Fig. 2. A new biologically motivated computational model of short-term memory is implemented through the interaction of neural and astrocytic networks. The model acts at multiple timescales: at a millisecond scale of firing neurons and the second scale of calcium dynamics in astrocytes. The neuronal network consists of randomly sparsely connected excitatory and inhibitory spiking neurons with plastic synapses. To train synapses in neural networks, we used the traditional STDP rule. Astrocytes track the neural activity and respond to it by intracellular calcium elevations, which trigger the release of gliotransmitters. Gliotransmitter-induced short-term synaptic plasticity results in local spatial synchronization in neuronal ensembles. The short-term memory realized by such astrocytic modulation is characterized by one-shot learning and is maintained for seconds. The astrocytic influence on the synaptic connections during the elevation of calcium concentration implements Hebbian-like synaptic plasticity differentiating between specific and nonspecific activations. Composed of two building blocks, e.g., fast-spiking neurons and slow astrocytes, the proposed memory architecture eventually demonstrated synergetic functionality in loading information. The readout of this memory by the neuronal block and storage is implemented by the astrocytes.

SNAN Architecture: The architecture of the proposed SNAN is shown in Fig. 3. The SNAN includes three interacting layers: the layer of pyramidal neurons, the layer of interneurons, and the astrocytic layer. An input signal encoded as 2-D patterns was applied to the first layer. The first layer consists of 6241 (79×79) synaptically coupled pyramidal neurons, which are connected randomly with their connection length determined by the exponential distribution. To maintain the balance of excitation and inhibition during neuronal activity, the layers of pyramidal neurons and interneurons communicate bidirectionally. Astrocytes generating calcium signals are connected by local gap junction diffusive couplings. To design the interaction of the neuronal and astrocytic layers, we followed the approach proposed in our previous works [35], [36]. Calcium elevations occur in response to the increased concentration of the neurotransmitter released by pyramidal neurons when a group of them fires coherently. In turn, gliotransmitters are released by activated astrocytes modulating the strength of the synaptic connections in the corresponding neuronal group. The output signal is taken from frequencies of transient discharges of pyramidal neurons.

Detailed information concerning the models and the description of parameters is provided in Section V.

V. Model Details

In this section, the SNAN architecture is described in detail together with the STDP learning rule and neuron/astrocytic models. Specifically, we start with biological realistic models of neuronal, astrocytic networks that capture the essence of the biological interplay between these cells, at the same time minimizing the computational overhead. Then, we describe the communication between pyramidal neurons and astrocytes at tripartite synapses.

1) Neural Network: Among the many existing biological plausible spiking neuron models [37], [38], [39], [40], we have chosen the simplified Izhikevich model [41] as computationally efficient for modeling networks. The

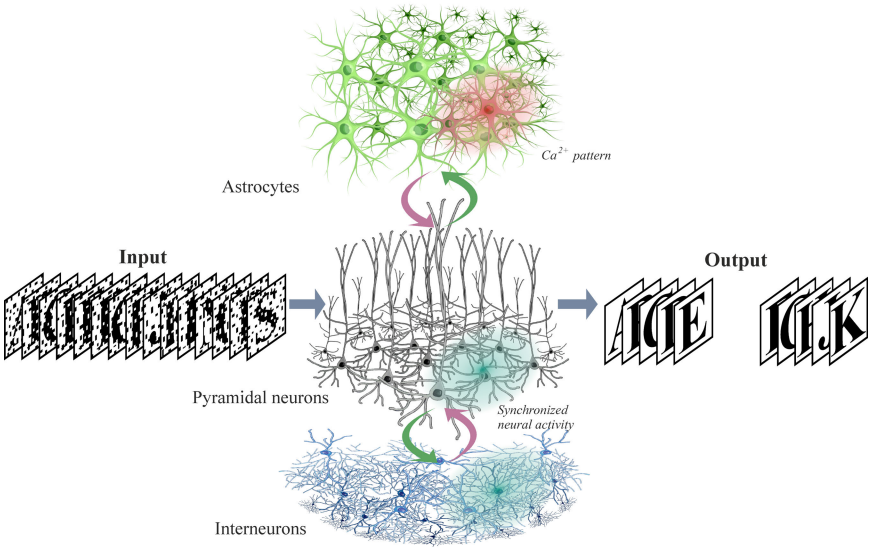

Fig. 2. Concept of the situation-based memory operation in the SNAN model.

dynamics of neuronal membrane potential are given by [41]

$$\begin{aligned}\frac{dV_i}{dt} &= 0.04V_i^2 + 5V_i - U_i + 140 + I_{\text{app},i} + I_{\text{syn},i}\\ \frac{dU_i}{dt} &= a(bV_i - U_i)\end{aligned} \tag{1}$$

with the auxiliary after-spike resetting

$$\text{if } V_i \geq 30 \text{ mV, then } \begin{cases} V_i \leftarrow c \\ U_i \leftarrow U_i + d \end{cases} \tag{2}$$

where the subscript i corresponds to the neural index, V_i is the neuronal membrane potential in millivolts, and time t in milliseconds. The applied current $I_{\text{app},i}$ simulates the input signal, $I_{\text{syn},i}$ is the synaptic current. The parameter descriptions and their values used in this work can be found in Table S1 of the supplementary material.

The total synaptic current injected from all synapses of ith neuron is described by [42], [43]

$$I_{\text{syn},i} = \sum_{k=1}^{N_i} \frac{w_{\text{syn},k}(E_{\text{syn}} - V_i)}{1 + \exp(-V_{\text{pre},k}/k_{\text{syn}})} \tag{3}$$

where N_i is the total number of synapses, $w_{\text{syn},k}$ is the weight of the kth synapse associated with neuron, V_{pre} is the membrane potential of the presynaptic neuron, E_{syn} is the synaptic reversal potential. $E_{\text{syn}} = -90$ mV for the inhibitory synapse and $E_{\text{syn}} = 0$ mV for the excitatory. Parameter k_{syn} denotes the slope of the synaptic activation function threshold. We neglect the synaptic and axonal delays in the system for simplicity.

Pyramidal neurons interact with each other (connection type: EE) and with interneurons (EI). Interneurons communicate with pyramidal neurons (IE) and are not interconnected. The architecture of synaptic connections between neurons is nonspecific (random) with different parameters within excitatory and inhibitory layers, as well as between layers, which is described further below. A detailed list of parameter values of synaptic connection organization can be found in Table S1 of the supplementary material. The number of output connections per each neuron is fixed at N_{out}. Each postsynaptic neuron is randomly selected in polar coordinates. The distances between neurons r are determined by the exponential distribution $f_R(r)$, and the angles ϕ are chosen from a uniform distribution in the range $[0; 2\pi]$

$$f_R(r) = \begin{cases} 1/\lambda \exp(-r/\lambda), & r \geq 0 \\ 0, & r < 0. \end{cases} \tag{4}$$

Considering the difference in the sizes of the layers, the coordinates of postsynaptic neurons are calculated as follows:

$$\begin{aligned}\text{EE: } x_{\text{post}} &= \lceil x_{\text{pre}} + r\cos(\phi) \rceil \\ y_{\text{post}} &= \lceil y_{\text{pre}} + r\sin(\phi) \rceil \\ \text{EI: } x_{\text{post}} &= \lceil K_1^{-1} x_{\text{pre}} + r\cos(\phi) \rceil \\ y_{\text{post}} &= \lceil K_2^{-1} y_{\text{pre}} + r\sin(\phi) \rceil \\ \text{IE: } x_{\text{post}} &= \lceil K_1 x_{\text{pre}} + r\cos(\phi) \rceil \\ y_{\text{post}} &= \lceil K_2 y_{\text{pre}} + r\sin(\phi) \rceil \end{aligned} \tag{5}$$

where x_{pre} and y_{pre} denote the coordinates of the presynaptic neuron, x_{post} and y_{post} are the coordinates of the postsynaptic neurons, $K_1 = W/W_1$, $K_2 = H/H_1$. Coordinates are picked repeatedly in case of duplicated connection (random selection was a process without replacement).

In the proposed SNAN, the synaptic weights dynamically adjust during training only for EE and IE types of synaptic connections. The synaptic weights for EI synapses are fixed and equal to $w_{\text{synEI}} = 0.1$. The initial weights of the synapses between pyramidal neurons (EE) and interneuron–pyramidal neurons (IE) are 10^{-4}. The maximum weights are limited to values $w_{\text{synEEmax}}, w_{\text{synIEmax}}$. The STDP rule updates the synaptic weights according to the timing difference between the pre and postsynaptic spikes and is described by

$$\delta w_{\text{synEE},k}(\Delta t) = \begin{cases} g_{\text{synEE}} \exp(\Delta t/\tau), & \Delta t \leq 0 \\ -g_{\text{synEE}} \exp(\Delta t/\tau), & \Delta t > 0 \end{cases}$$
$$w_{\text{synEE},k} \in [10^{-4}, w_{\text{synEEmax}}] \tag{6}$$

where $\delta w_{\text{synEE},k}(\Delta t)$ is used to update the synaptic weight, Δt is the time difference between presynaptic and postsynaptic

spikes, g_{synEE} is the plasticity window height, τ control the width of the plasticity window, and they are 20 ms in our model. Training of synaptic connections from interneurons to pyramidal neurons is organized so that interneurons activated by pyramidal neurons inhibit all subnetworks of pyramidal neurons that were not active during the presentation of the training pattern. In such a way, the weights of IE synapses are updated according to the following:

$$\delta w_{\text{synIE},k}(\Delta t) = \begin{cases} g_{\text{synIE}} \exp(\Delta t/\tau) H(f^* - f), & \Delta t \le 0 \\ -g_{\text{synIE}} \exp(\Delta t/\tau), & \Delta t > 0 \end{cases}$$
$$w_{\text{synIE},k} \in [10^{-4}, w_{\text{synIEmax}}] \quad (7)$$

where Δt is the time difference between presynaptic and postsynaptic spikes, g_{synIE} is the plasticity window height, τ control the width of the plasticity window, and they are 20 ms in our model. f and f^* are the actual firing rate (i.e., a running average over 10 ms) and threshold firing rate of the postsynaptic pyramidal neuron, respectively. H is the Heaviside step function.

2) Astrocytic Network: The astrocytic layer consists of 676 cortical astrocytes connected with only nearest neighbors. It has been experimentally shown that individual cortical astrocytes contact several neuronal somatas and hundreds of neuronal dendrites with some overlapping in the spatial territories corresponding to different astrocytes in the cortex [44]. Such an organization of neuron-astrocyte interaction allows the astrocytes to integrate and coordinate a unique volume of synaptic activity. Following experimental evidence, each astrocyte in the SNAN bidirectionally interacts with an ensemble of $N_{\text{AE}} = 16$ pyramidal neurons with some overlapping. Spiking neuronal activity induces the release of neurotransmitters (glutamate) from the presynaptic terminals into the synaptic gap. The released glutamate binds to the metabotropic glutamate receptors (mGluRs) on the astrocyte membrane and triggers the production of inositol 1,4,5-trisphosphate (IP_3) in astrocytes, which is followed by the generation of a calcium pulse. The Ullah model [45] is used to describe the dynamics of the intracellular concentrations of IP_3 and Ca^{2+} in astrocytes

$$\begin{aligned} \frac{d[\text{Ca}^{2+}]_m}{dt} &= J_{\text{ER}} - J_{\text{pump}} + J_{\text{leak}} + J_{\text{in}} - J_{\text{out}} + J_{\text{Gca}} \\ \frac{dh_m}{dt} &= a_2\left(d_2 \frac{[\text{IP}_3]_m + d_1}{[\text{IP}_3]_m + d_3}(1 - h_m) - [\text{Ca}^{2+}]_m h_m\right) \\ \frac{d[\text{IP}_3]_m}{dt} &= \frac{[\text{IP}_3]^* - [\text{IP}_3]_m}{\tau_{\text{IP3}}} + J_{\text{PLC}\delta} + J_{\text{glu}} + J_{\text{Gip3}} \end{aligned} \quad (8)$$

where m ($m = 1, \ldots, 676$) is the astrocyte index. $[Ca^{2+}]$, $[IP_3]$, h are the cytosolic calcium and IP_3 concentrations and fraction of activated IP_3 receptor on the endoplasmic reticulum (ER) membrane, respectively. J_{ER} is Ca^{2+} flux from the ER to the cytosol, J_{pump} is the pump flux from the cytosol to ER, and J_{leak} is the leakage flux from the ER to the cytosol. The fluxes J_{in} and J_{out} describe the exchange of calcium with the extracellular space. $J_{\text{PLC}\delta}$ describes the production of IP_3 by phospholipase Cδ (PLCδ), J_{glu} describes the glutamate-induced IP_3 production in response to neural activity. These fluxes are expressed as follows:

$$\begin{aligned} J_{\text{ER}} &= c_1 v_1 [\text{Ca}^{2+}]^3 h^3 [\text{IP}_3]^3 \frac{\left(c_0/c_1 - (1 + 1/c_1)[\text{Ca}^{2+}]\right)}{\left(([\text{IP}_3] + d_1)([\text{Ca}^{2+}] + d_5)\right)^3} \\ J_{\text{pump}} &= \frac{v_3 [\text{Ca}^{2+}]^2}{k_3^2 + [\text{Ca}^{2+}]^2} \\ J_{\text{leak}} &= c_1 v_2 \left(c_0/c_1 - (1 + 1/c_1)[\text{Ca}^{2+}]\right) \\ J_{\text{in}} &= \frac{v_6 [\text{IP}_3]^2}{k_2^2 + [\text{IP}_3]^2} \\ J_{\text{out}} &= k_1 [\text{Ca}^{2+}] \\ J_{\text{PLC}\delta} &= \frac{v_4 \left([\text{Ca}^{2+}] + (1 - \alpha) k_4\right)}{[\text{Ca}^{2+}] + k_4}. \end{aligned} \quad (9)$$

Astrocytes interact with each other through gap junctions. Gap junctions are permeable to the second messenger IP_3 and to calcium ions [46], [47]. Currents J_{Gcam} and J_{Gip3m} describe the diffusion of Ca^{2+} ions and IP_3 molecules via gap junctions of the mth astrocyte and can be expressed as follows:

$$\begin{aligned} J_{\text{Gcam}} &= d_{\text{ca}} \sum_j ([\text{Ca}^{2+}]_j - [\text{Ca}^{2+}]_m) \\ J_{\text{Gip3m}} &= d_{\text{ip3}} \sum_j ([\text{IP}_3]_j - [\text{IP}_3]_m) \end{aligned} \quad (10)$$

where j, d_{ca}, and d_{ip3} represent, respectively, the number of astrocytes connected to the mth astrocyte and the Ca^{2+} and IP_3 diffusion rates. Biophysical meaning of all parameters in (8)–(10) and their values can be found in [45] and are summarized in Table S2 of the supplementary material (astrocytic network parameters). Note that the timescale of the model of calcium dynamics in astrocytes is seconds. At the same time, the timescale of model (1), (2) is milliseconds. To match the timescales in the combined model, we had to appropriately rescale the values of relevant model parameters.

3) Bidirectional Neuron-Astrocyte Interaction: The amount of neurotransmitter-glutamate that diffuses from the synaptic cleft associated with the ith pyramidal neuron and reaches the astrocyte is described by the following equation [25], [48]:

$$\frac{dG_i}{dt} = -\alpha_{\text{glu}} G_i + k_{\text{glu}} H(V_i - 30 \text{ mV}) \quad (11)$$

where α_{glu} is the glutamate clearance constant, k_{glu} is the release efficiency, H is the Heaviside step function, and V_i is the membrane potential of ith pyramidal neuron. Glutamate contacts the mGluRs on the astrocyte membrane and initiates the production of IP_3. The flux J_{glu} represents the glutamate-induced IP_3 production and is defined as follows:

$$J_{\text{glu}} = \begin{cases} A_{\text{glu}}, & \text{if } t_0 < t \le t_0 + t_{\text{glu}} \\ 0, & \text{otherwise} \end{cases} \quad (12)$$

here t_0 represents the moment when the total level of glutamate concentration in all synapses associated with this astrocyte reaches a threshold

$$\left(\frac{1}{N_{\text{AE}}} \sum_{i \in N_{\text{AE}}} [G_i \ge G_{\text{thr}}]\right) \ge F_{\text{act}} \quad (13)$$

where the parameter $G_{\text{thr}} = 0.2$ is the threshold for glutamate, $[x]$ is the Iverson bracket. $F_{\text{act}} = 0.75$ denotes the fraction

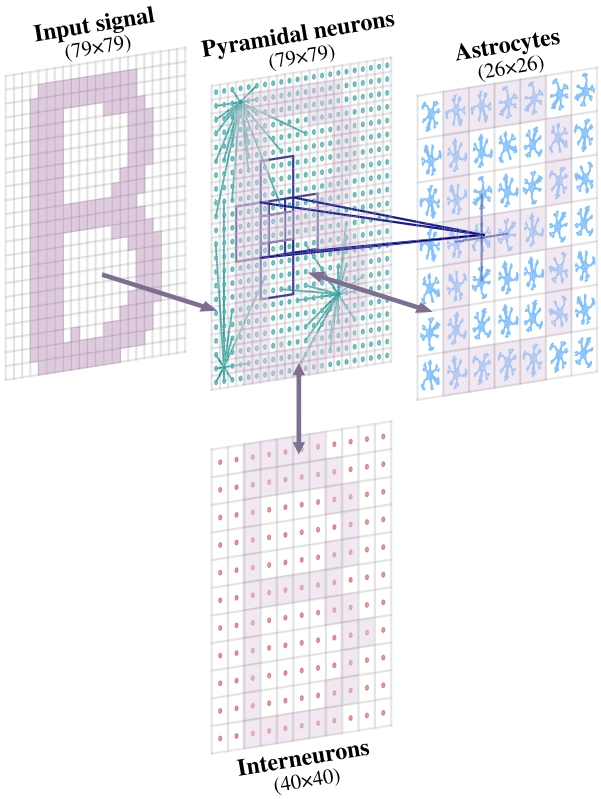

Fig. 3. SNAN topology. The SNAN includes three interacting layers: the layer of pyramidal neurons, the layer of interneurons, and the astrocytic layer. The first layer (79 × 79) consists of synaptically coupled pyramidal neurons. The pyramidal neurons bidirectionally communicate with the interneurons from the second layer (40 × 40). The ratio of pyramidal neurons to interneurons in the model is chosen in accordance with the experimental observations and computational model of the cortex [54], where 80% of the CSN neurons are pyramidal neurons and 20% are interneurons. Astrocytes are connected by a local gap junction diffusive couplings and represent a 2-D square lattice with a dimension 26 × 26. We focus on the bidirectional interaction between the first neuronal and astrocytic layers. Each astrocyte is interconnected with an ensemble of $N_a = 16$ pyramidal neurons with dimensions 4 × 4 (red lines) overlapping in one row and one column. An input signal encoded as a 2-D pattern is applied to the first layer.

of synchronously spiking neurons of the neuronal ensemble corresponding to the astrocyte.

Experimental studies have shown that astrocytes are able to facilitate synaptic transmission due to the action of glutamate released from astrocytes. More precisely, we consider that the astrocytic glutamate induces potentiation of the excitatory synapse via NMDAR-dependent postsynaptic slow inward currents (SICs) generation [49], [50] and mGluR-dependent heterosynaptic facilitation of presynaptic glutamate release [51], [52], [53]. In the SNAN, we propose that Ca^{2+} elevation in astrocytes results in glutamate release, which can modulate the synaptic strength of all synapses corresponding to the morphological territory of a given astrocyte. For simplicity, astrocyte-induced enhancement of synaptic weight of the affected excitatory synapses, $\overline{w_{\text{synEE}}}$, is described as follows:

$$\begin{aligned} \overline{w_{\text{synEE}}} &= w_{\text{synEE}}\ (1+\nu_{\text{Ca}}), \quad w_{\text{synEE}} \in [0, w_{\text{synEEmax}}] \\ \nu_{\text{Ca}} &= \nu^*_{\text{Ca}} H\left([\text{Ca}^{2+}]_m - [\text{Ca}^{2+}]_{\text{thr}}\right) \end{aligned} \tag{14}$$

where w_{synEE} is the weight of the excitatory synapse trained according to Hebb's rule, $\nu^*_{\text{Ca}} = 2$ represents the strength of the astrocytic modulation of the synaptic weight, $H(x)$ is the Heaviside function, $[\text{Ca}^{2+}]_{\text{thr}}$ denotes the threshold Ca^{2+} concentration in the astrocyte m. The feedback from the astrocytes to the neurons is activated when the astrocytic Ca^{2+} concentration is larger than $[\text{Ca}^{2+}]_{\text{thr}}$, and the fraction of synchronously spiking neurons of neuronal ensemble corresponding to the astrocyte F_{astro} during the period of $\tau_{\text{syn}} = 5$ ms. The duration of astrocyte-induced enhancement of synaptic transmission is fixed and equal to $\tau_{\text{astro}} = 20$ ms.

Model equations are integrated using the Runge–Kutta fourth-order method with a fixed time step, $\Delta t = 0.1$ ms. A detailed listing of model parameters and values can be found in Tables S1 (neural network model) and S2 (astrocytic network and neuron-astrocytic interaction) of the supplementary material. The code is available at https://github.com/altergot/Neuron-astrocyte-network-Situation-associated-memory.

VI. Memory Performance Metrics

For a detailed description of the algorithm used to measure the memory performance of the proposed SNAN, please refer to the supplementary materials.

Training and Testing Protocol: To train and test the proposed SNAN, we use the alpha-digits dataset (https://github.com/altergot/Neuron-astrocyte-network-Situation-associated-memory/tree/main/images) which consists of P binary images of digits and capital letters of size $W \times H$ pixels. The input patterns are fed to the layer of pyramidal neurons. Each image pixel corresponds to a neuron, which receives a rectangular excitatory pulse, $I_{\text{app},i}$, with length t_{stim} and amplitude A_{stim} for training (with t_{test} and A_{test} in case of testing). On average there are 950 neurons under stimulation (15% of the network) in a training image. Training samples were presented to highly overlapped neuronal populations (an average for 40 training samples overlapping was 51%). The output signal was read out according to the firing rates of pyramidal neurons. Table S3 in the supplementary material provides a list of the training and testing protocol parameters and their corresponding values.

1) SNN Pretraining: First, we pretrained the synaptic connections only in the spiking neuronal network consisting of pyramidal neurons and interneurons without taking into account the influence of astrocytes. During pretraining, each of the P patterns was presented to the neuronal network ten times in random order. After the pretraining was completed, the network weights were fixed. To test the training quality, we calculated the correlation of recalled patterns with the ideal samples according to the procedure described in Section VI. In the cued recall, we applied a shorter input with lower amplitude (t_{test} and A_{test}) to the network. These inputs were spatially distorted by high-level random noise matching the training samples.

2) Situation-Based Learning in SNAN: To implement the situation-based learning in the proposed SNAN, we use the following protocol. After the SNN pretraining, we turn on the bidirectional interaction between the pyramidal neuron layer and the astrocytic layer. To let the astrocytic network generate the first calcium pattern, we apply the initial pool of patterns to SNAN. This pool consists of seven randomly

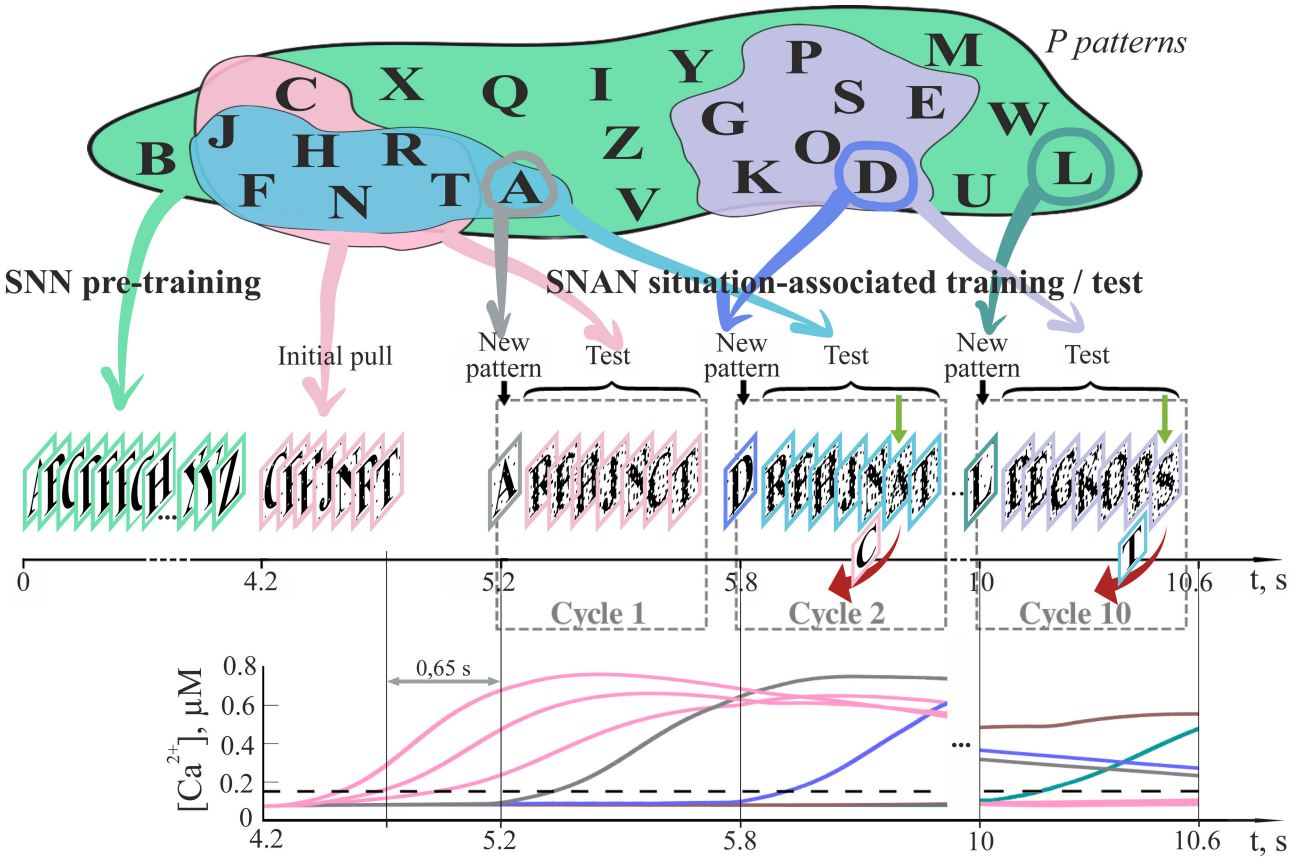

Fig. 4. Training and testing protocol. For training and testing of the proposed SNAN, we use the alpha-digits dataset consisting of P binary images of digits and capital letters. The input patterns are fed to the layer of pyramidal neurons. First, we pretrain the spiking neuronal network consisting of pyramidal neurons and interneurons without considering the influence of astrocytes. During pretraining, each P pattern is presented to the neuronal network ten times in random order (green). After the pretraining is completed, the synaptic weights are fixed. To implement the situation-based learning in the proposed SNAN, we use the following protocol. After the SNN pretraining, we turn on the bidirectional interaction between pyramidal neurons and astrocytic layers. To let the astrocytic network generate the first calcium pattern, we apply the initial pool of patterns to SNAN. This pool consists of seven randomly selected patterns (pink) from the general dataset used in the SNN pretraining. Each pattern is presented ten times with the addition of a random 5% "salt and pepper" noise. After a break (approximately 650 ms) necessary for the formation of calcium elevations in the pattern-specific astrocytes (examples of astrocytic Ca^{2+} signals are shown in colors corresponding to the patterns), we start the ongoing training-testing process of the SNAN in real-time. This situation-based learning process can be conventionally divided into a sequence of cycles, which follow each other continuously. Every test cycle starts with the training of the SNAN on one new pattern (e.g., pattern "A," gray), which was absent in the initial pool and was randomly chosen from the general dataset. After that, we test the memorization of all patterns from the initial pool—"Cycle 1." We present the SNAN with test patterns that have been spatially distorted by high-level noise. To identify the memory performance, we analyze the quality of the recalled patterns. In the next cycle, "Cycle 2," one pattern from the initial pool (pattern "C") is replaced by a new pattern that has been learned in the previous cycle (pattern "A"), which models a situation-based environment. Thus, after N cycles all patterns from the initial pool are substituted by new patterns from the general pretraining dataset. This procedure can be performed endlessly allowing the system to work with all patterns from the general dataset in situation-based mode.

selected patterns from the general dataset used in the SNN pretraining. Each pattern was presented ten times.

Noise is an essential part of both sensory input [55] and internal neuronal dynamics and may contribute to information processing in neural systems as well as to learning and memory [56]. Noise can play the role of a regularizer in training deep learning neural networks too [57]. Recent work demonstrated that external noise in SNN-based learning systems could help to maintain and recover memorized patterns [58]. Given the ubiquity and relevance of noise, we corrupted the input training patterns by a random 5% "salt and pepper" noise. After a break (approximately 650 ms) needed for the formation of calcium impulses in pattern-associated astrocytes, we started the ongoing training-testing process of the SNAN in real-time. This situation-based learning process can be conventionally divided into a sequence of cycles, which follow each other continuously.

Every test cycle starts with training of the SNAN on one new pattern which was absent in the initial pool and was randomly chosen from the general dataset. After that, we test the storage of all patterns from the initial pool in memory. Throughout the article, we use the term 'memory' to refer to the ability of pattern recall in the presence of perturbations. We present the SNAN with the seven test patterns that match the patterns from the initial pool but have shorter lengths, lower amplitude (t_{test} and A_{test}), and which are spatially distorted by high level (20%) random noise. To identify the memory performance, we analyze the quality of the recalled patterns. In the next cycle, one pattern from the initial pool is replaced by a new pattern that has been learned in the previous cycle. Thus, after seven cycles all patterns from the initial pool are substituted by new patterns from the general pretraining dataset. This procedure can be performed endlessly allowing the system to work with all patterns from the general dataset

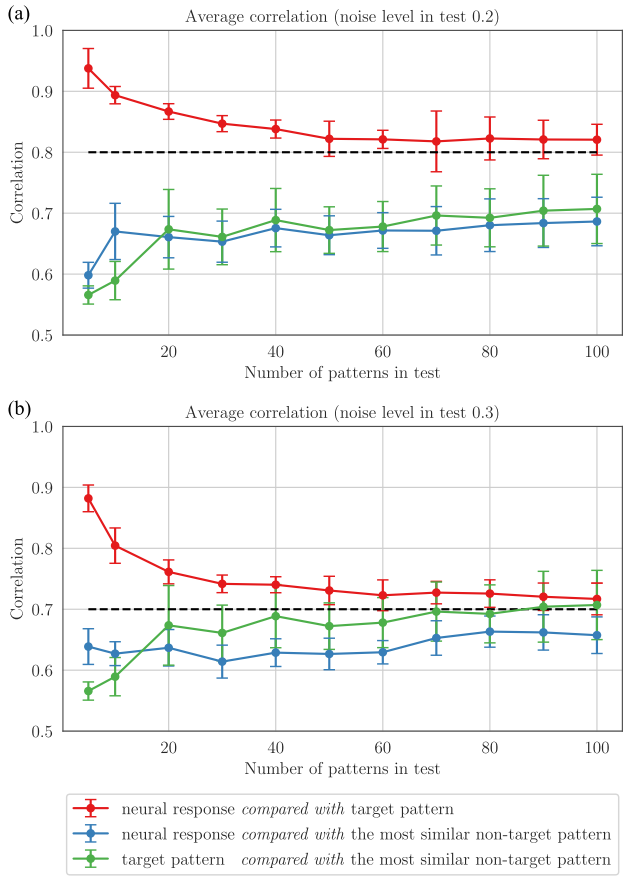

Fig. 5. Pretrained SNN's memory performance. The correlations between SNN recalls and the ideal target samples for different dataset sizes are marked in red. The maximum correlations between SNN recalls and nontarget samples are marked in blue. The maximum correlation between target and nontarget samples are marked by green. Average means over all test patterns ± standard deviation are shown for (a) 20% and (b) 30% noise levels in test images. The dotted line indicates test patterns correlation.

in a situation-based mode. Fig. 4 shows the time scheme of the training and testing protocol.

VII. Results

A. SNN Memory Performance

First, we determine the size of the general dataset that can be loaded in memory of the SNN and used for implementation of the situation-based learning in the proposed SNAN. For this, we pretrain the SNN on the dataset of different sizes and test the quality of memory maintenance of the SNN in cued recall. Information retrieval is organized by the application of a cue sample representing one pattern from the memory set distorted by "salt and pepper" noise. The dependencies of the correlation between the SNN cued recalls and the ideal target samples (averaged over all test patterns ± standard deviation) on the dataset size are shown in Fig. 5 by red curves. Two cases were considered for test images distorted by 20% [Fig. 5(a)] and 30% [Fig. 5(b)] noise levels. The maximum correlations between SNN recall and nontarget samples averaged over all test patterns and the maximum correlation between the target and nontarget samples are presented by blue and green curves in Fig. 5, respectively. According to the results obtained, the considered SNN can learn up to 40 patterns. In further

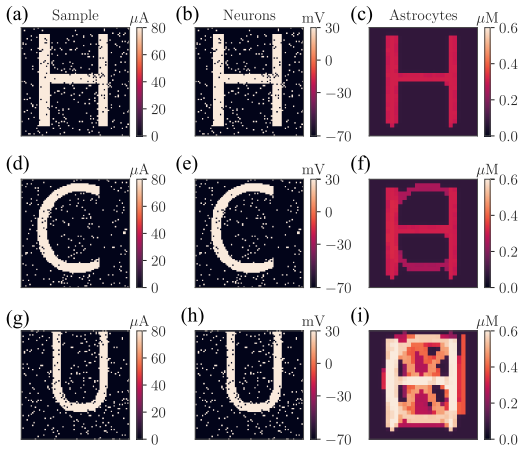

Fig. 6. Example of SNAN training on the patterns from the initial pool (Fig. 4). (a), (d), and (g) First, second, and seventh training patterns from the initial pool, respectively. (b), (e), and (h) Responses of the pyramidal neuronal layer to the patterns. The values of the membrane potentials are shown. (c), (f), and (i) Intracellular Ca^{2+} concentrations in the astrocytic layer.

analysis, we used dataset sizes of 20 and 40 patterns for comparison.

B. SNAN Situation-Based Learning Performance

1) Astrocytic Contribution to the SNAN Memory Performance: To assess the contribution of astrocytes in information processing and memory formation in neuron-astrocyte networks, the pretrained SNN was bidirectionally connected to the astrocytic layer. To start the process of the SNAN situation-based learning, we load the initial pool of seven patterns to the system by applying the inputs [Fig. 6(a), (d), and (g)] to the pyramidal neuronal layer. The activity of pattern-specific neuronal subnetworks [Fig. 6(b), (e), and (h)] induces the generation of calcium signals in corresponding astrocytes. Due to the fact that calcium dynamics in astrocytes has slow scale, the overlapped spatial calcium patterns in astrocytic layer for different samples coexist for several seconds [Fig. 6(c), (f), and (i)].

Then, we ran the ongoing process of situation-based learning according to the approach described in Section VI-2 and shown in Fig. 4. Briefly, in each of the ten cycles, we loaded a new pattern from pretraining dataset to the SNAN and tested the patterns memorized in the previous cycles. A constant number of patterns in the cycle was maintained by deleting one randomly selected pattern during each cycle. Test patterns were applied to the pyramidal neurons with 20% level noise, and the SNANs cued recalls in the values of the neuronal firing rate were read out. Examples of input test images from several cycles and the systems retrievals are shown in Fig. 7.

To estimate the astrocytic impact on memory formation in the SNAN, we calculated the dependencies of recall correlation with samples on the noise level. First, the test was run with astrocytic modulation of synaptic transmission in the SNN and then without it (Fig. 8). The test involved 20 and 40 patterns from the pretrained dataset. The differences in correlation between the recalled pattern and noisy input clearly show that astrocytes steadily improve the quality of the system retrieval up to 10% for high noise levels (red curve

Fig. 7. Example of the SNAN test patterns from the general pretrained dataset (Fig. 4). Three testing cycles are shown. (Left) Testing images with 20% "salt-and-pepper" noise. (Right) Cued recalls in the pyramidal neuronal layer. The averaged firing rate on the test time interval for each neuron is shown.

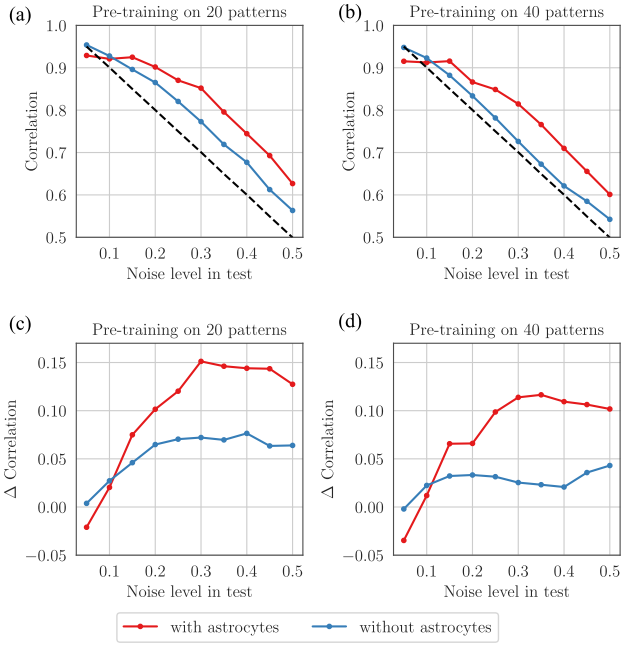

Fig. 8. Astrocyte-induced enhancement of the memory performance in the proposed SNAN. (a) and (b) Correlations between SNAN recalls and the ideal samples dependent on noise level in testing patterns with astrocytic modulation of synaptic transmission in neural networks (red curves) and without it (blue curves). (c) and (d) Difference between correlations of systems recalls and test patterns. (a) and (c) and (b) and (d) correspond to dataset sizes of 20 and 40 patterns, respectively. The dotted line indicates test patterns correlation.

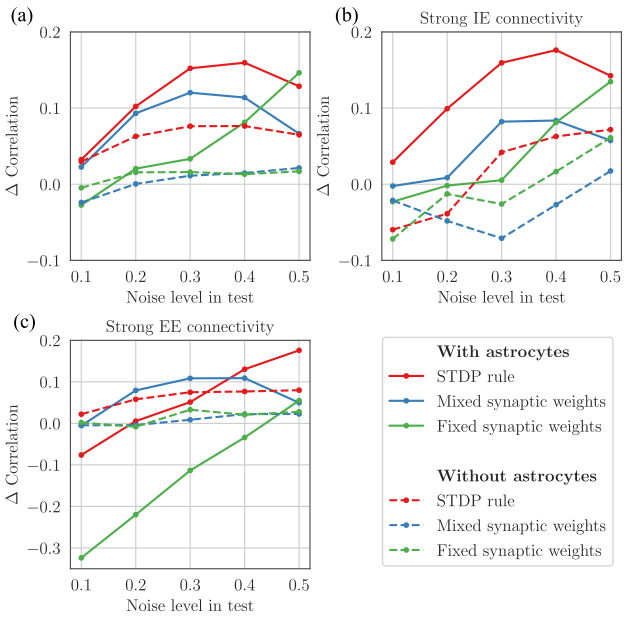

Fig. 9. Difference between correlations of the SNANs recalls and test patterns. The memory performance was shown for three SNAN types with and without astrocytic influence: 1) with synaptic connections trained according to the STDP rule; 2) with randomly mixed synaptic weights after the SNN pretraining; and 3) with fixed synaptic weights without the SNN pretraining. (a) $w_{\text{synIEmax}} = 0.05$, $w_{\text{synEEmax}} = 0.05$. (b) Strong connections from interneurons to pyramidal neurons $w_{\text{synIEmax}} = 0.15$, $w_{\text{synEEmax}} = 0.05$. (c) Strong connections inside the pyramidal neurons layer $w_{\text{synIEmax}} = 0.05$, $w_{\text{synEEmax}} = 0.07$.

in comparison with blue curve). The reason for such recall enhancement is that a short presentation of the cue to the neural network evokes the additional astrocytic-induced spike in the synaptic strength between stimulus-specific neurons, which results in a local spatial synchronization in the whole stimulus-specific neuronal population.

2) Contribution of the SNN Pretraining to the SNAN Memory Performance: Next, we evaluate the contribution of neural network learning to the SNAN memory performance according to synaptic weights adjustment via the STDP rule. For this, we compare the memory performance of the three SNAN types: 1) with synaptic connections trained according to the STDP rule; 2) with randomly mixed synaptic weights after the SNN pretraining, and 3) with fixed synaptic weights without the SNN pretraining. Fig. 9(a) shows the changes in the correlation of the SNANs cued retrievals relative to the input noise patterns for these cases with and without astrocytic influence on neural activity. The best levels of recall correlations were demonstrated by the proposed SNAN trained by the STDP rule with astrocytic modulation of synaptic transmission, followed by the SNAN with mixed synaptic weights and astrocytic modulation, and then the pretrained SNN without astrocytes. The worst results were shown by networks without astrocytic modulation of synaptic transmission and without training of synaptic connections. Interestingly, astrocyte-induced enhancement of synaptic transmission in the sample-specific neuronal subnetworks can provide good quality retrieval in the system even for neural networks with mixed weights of synaptic connections [blue line in Fig. 9(a)].

3) Effect of the Synaptic Connectivity Strength on the SNAN Memory Performance: Next, we studied the influence of synaptic connectivity architecture in the neural layers of the SNAN on the correlation of the system recalls. We specifically focused on the weight of synaptic connections between layers

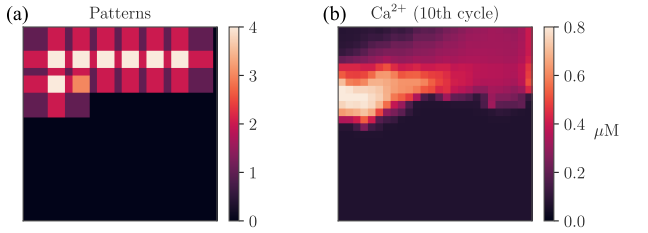

Fig. 10. (a) Example of the dataset used for evaluation of the impact of the samples overlapping on the SNAN memory performance. The figure shows the case for samples of size 17×17 pixels with overlapping in 7 pixels which corresponds to overlapping in 41.18% between the neighboring patterns. (b) Corresponding calcium activity in an astrocytic layer.

and inside the pyramidal neuronal layer. Higher inhibition of the system [Fig. 9(b)] due to the increase of the maximum synaptic weights of the connection from interneurons layer to pyramidal neurons, w_{synIEmax}, induces the SNN memory performance decline (red dashed line), but does not affect the SNAN memory performance (red line). This can be explained by the fact that samples in training were applied to highly overlapped neuronal populations. Such subnetworks of interneurons corresponding to several patterns provide strong inhibition of the signal propagation in a sample-specific population of pyramidal neurons and prevent correct recall. However, this can be compensated by the stimuli-specific astrocyte-induced enhancement of excitatory synaptic transmission. On the contrary, increasing the maximum excitatory synaptic strengths in the pyramidal neuronal layer, w_{synEEmax}, results in astrocyte-induced overactivation of the SNAN and a decrease in the recall quality (Fig. 9(c) red and green lines).

4) Capacity of the Situation-Based Memory in the SNAN: The situation-based memory capacity in the proposed SNAN is determined by the duration of Ca^{2+} signals in astrocytes. Duration of astrocytic Ca^{2+} elevations is determined by the intrinsic mechanisms of the IP_3-evoked calcium release from the ER in astrocytes, which is described by the biophysical model [45] used in this study. Brief application of the cue samples during testing results in prolongation of Ca^{2+} elevations in astrocytes and, thus, in the increased storage time of patterns in the memory of the SNAN. On average, the Ca^{2+} signals duration in astrocytes is 3.8 s, which can support the situation-based learning during nine cycles on 15 different patterns.

5) Impact of the Overlapping Level in Samples on the SNAN Memory Performance: The pretrained spiking neural network can retrieve the correct samples from test images distorted with 20% noise level with an average correlation level of 96%. This, however, applies only to nonoverlapping patterns without additional effect of astrocytic modulation, since even a small sample overlapping results in chimeras generation in the solely neuronal network model. To characterize the impact of the overlapping level in training samples on the SNAN memory performance, we use rectangles of different sizes displaced at the fixed number of pixels relative to the neighbor as information patterns [Fig. 10(a)]. In this case, in contrast to the used alpha-digit dataset, the level of overlap between the neighboring patterns can be precisely specified.

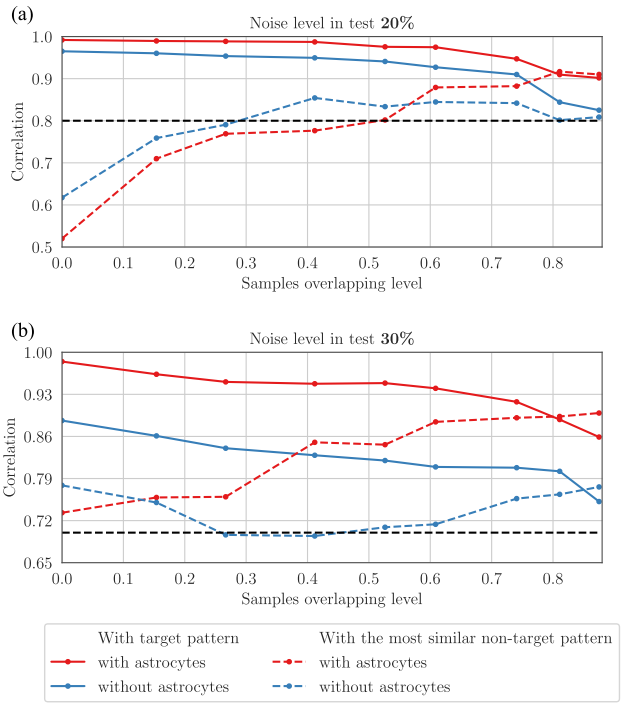

Fig. 11. Impact of the overlapping level in samples on the SNAN memory performance. The dependencies of correlation level of the SNANs cued recalls and samples for different levels of sample overlapping are shown for SNAN with astrocytic modulation of synaptic transmission and without it for (a) 20% and (b) 30% noise level. Blue and red dotted lines show a correlation of system recalls with the most similar nontarget samples. Black dotted lines indicate test patterns correlation.

After the SNN pretraining on 40 patterns with fixed overlapping, we use the situation-based training and testing protocol for the SNAN described above with little modifications. To be sure that the sample overlapping level inside one cycle is constant between all patterns, we apply samples to the SNAN sequentially (not in random order as before). The example of corresponding calcium activity in an astrocytic layer is shown in Fig. 10(b). The dependencies of correlation level of the SNANs cued recalls on different overlapping levels of samples are shown in Fig. 11 for SNAN with astrocytic modulation of synaptic transmission and without it. Results show that including the astrocytic modulation of synaptic transmission into a spiking neural network with connections trained according to the Hebbian plasticity leads to a robust improvement of the system retrieval performance for almost all levels of sample overlapping, excluding the highest levels (>80%). It is important to note that the contribution of astrocytes is especially significant for a high noise value in cue samples [comparing Fig. 11(a) with (b)]. On average, in the range of samples with overlapping levels from 0 to 0.9, the astrocyte-induced enhancements of retrieval quality (in particular, the correlation of cued recalls with ideal samples) amounts to 5% for test samples distorted by 20% noise and 20% for −30% noise in cue samples. Fig. 11 shows that even for huge pattern overlapping, spurious correlations never dominate in that sense as the accuracy of our system is always equal to 100%. Correlation with the target sample always exceeds correlation with the wrong sample.

6) Comparative Analysis: For comparative analysis, we summarized the performance of the situation-based memory in the developed SNAN and also that of other published studies on the short-term working memory in the SNNs with biologically relevant unsupervised learning rule, such as STDP, in Table S3 of the supplementary material. Obviously, our result is one of the best in terms of frequency of target pattern activation. The developed SNAN is the only one that can deal with patterns presented to the overlapped neuronal populations, to the best of our knowledge.

To compare our results with the previous studies of the SNN-based classification methods, SNAN is trained and tested on the standard MNIST dataset (https://github.com/teavanist/MNIST-JPG) within the proposed situation-based memory framework. The dataset used in experiments was partitioned into the training and test sets comprising 10 000 and 2000 samples of 28×28 pixels images of digits 0–9, respectively. Original images from the MNIST dataset have been converted into 79×79 patterns to ensure consistency with the size of the pyramidal neuron layer. The SNN was pretrained on 10 000 training samples distorted by 5% noise applied to the rescaled images with one presentation of the sample. After the SNN pretraining, we trained the SNAN on the initial pool (containing 69 images in total, 3 digits $\times$ 23 images) using the proposed situation-based learning approach. The MNIST test images presented to the SNAN were corrupted with 20% noise applied to the rescaled images. During the ongoing training-testing process of the situation-based memory in our system in real-time, we calculated the correlations between recalls in the SNAN and the images from the MNIST training set. The average accuracy, measured as the proportion of instances when the pattern corresponding to the maximal correlation of SNAN recalls coincided with the target digit, is 97.2%. This compares favorably with the classification accuracy achieved in the previously reported SNN architectures.

Table S4 of the supplementary material summarizes the classification accuracies of the SNN-based systems with biologically plausible learning rules on the MNIST test set. Surprisingly, the pattern recognition system based on SNAN equipped with a simple correlator to process recalls appears to show higher accuracy than all other architectures presented in Table S4 of the supplementary material.

Using the procedure described above we also tested how the proposed situation-based memory in the SNAN can deal with the MNIST test set corrupted by correlated noise. A detailed description of these experiments and examples of the noisy test images along with the accuracy attained by the SNAN system in this task are provided in the supplementary material. Interestingly, in these additional experiments, the SNAN demonstrated good accuracy on test images distorted with high-level correlated noise without being shown any examples of images corrupted by such noise.

Comparing the proposed model with recent deep neural network (DNN) models in terms of memory performance can be highly intriguing. However, implementing deep-learning networks using spike-based frameworks is a topic that requires further research [59]. Such an approach is believed to be one of the primary challenges and future prospects of neuromorphic computing. Based on the results obtained thus far, the enrichment of spiking DNN models with astrocytic layers shows great promise. Conducting a comprehensive comparison of performance metrics between spiking DNN models with and without astrocytes would be highly interesting.

7) Relation to Transformer Models: Situation-based learning and inference implemented in the proposed SNAN model are closely related to the idea of attention. They also bear functional similarity to popular transformer models [12] in that both learning and inference are modulated by contexts inherent to particular situations evolving over time. SNANs' attention mechanism, implemented through astrocytes and relevant signaling pathways, is the consequence of the neuromorphic organization of the network (see [60]). This mechanism enables SNANs to exploit contexts, potentially over large temporal scales, whilst enjoying the benefits of parallel processing of information. The presence of attention circumventing the shortcomings of fixed network topology could explain why SNANs compare favorably to other relevant models, as is shown in Tables S3 and S4 of the supplementary material.

VIII. Discussion

The results obtained in the article could be instrumental in the development of brain-like (e.g., "strong") artificial intelligence. Inspired by the brain structural and functional organizational hierarchy, neuromorphic hardware systems that implement spike-driven computations could potentially be capable of implementing energy-efficient machine intelligence [59]. In addition, the possibility of enhancing learning performance by astrocytes is an important milestone in the ongoing discussion of the role of astrocyte-neuronal network interactions in brain processing [16]. Specifically, we have investigated the functional roles of different players, e.g., neurons, synapses, plasticity, and astrocytes, in the implementation of cognitive information-processing tasks in the brain. In particular, it was interesting to observe how the interplay of synaptic changes by STDP and by the gliotransmitter modulations improve memory performance (see Fig. 9).

The STDP-based plasticity represents a key biophysical mechanism of learning in neuronal networks and is considered one of the most perspective features for SNNs. Modeling and implementing this mechanism involves choosing appropriate values for its parameters. In this work, we did not intend to find optimal parameters of the STDP laws for SNNs as this was beyond the scope of our study. The main focus here was on exploring the holistic interaction between STDP, astrocytes, and neural dynamics in situation-based learning. Nevertheless, we recognize the importance of selecting parameters of STDP-based plasticity appropriately and would therefore like to refer interested readers to relevant literature on the topic [61], [62], [63].

In memory tasks, the synaptic weights are adjusted following a training protocol by sequential image application. Indeed, we also verified that STDP provided successful in training and information retrieval with a certain degree of

fidelity. In this context the interneurons balanced network firing by depression and, hence, we can safely assume that they are responsible for lateral inhibition via "selecting" stimulus-specific excitation routes. This solely neuronal story can not resolve the problem of "overlapping populations" when different input patterns stimulate similar neuronal groups (up to 50% of overlaps in our samples). Obviously, the synaptic plasticity alone can not resolve this problem, as it will inevitably lead to false recalls and decreased performance. However, our research shows that astrocytes can significantly improve this situation.

The astrocytic calcium operates at much slower time scales, hence, the astrocytes can not significantly affect the fast dynamics of neurons and synapses at the time scale of single image processing. Moreover, the calcium excitability has a gradual character [64]. It provides a proportional response to stimuli with different intensities. Thus, the stronger the activation of pyramidal neurons in terms of their discharge intensities over intervals of a dozen seconds, the higher the calcium response in the corresponding astrocytes. This way the astrocytes corresponding to the overlapping areas generate larger signals. In turn, they send back different levels of modulations during the recall processing. Furthermore, patterns with a high degree of overlap can be successfully resolved, which gives a noticeable increase in the retrieval fidelity.

At a functional level, astrocytes supplement neuronal processing by amplitude modulation in addition to rate encoding by all-or-none firing neurons. At the same time, being distributed in time the astrocytic modulation provides a dynamic separation of overlapping patterns. It is very similar to reservoir computing in machine learning with traditional artificial neurons [65], [66]. Here, the astrocytes serve as a reservoir naturally "predicting" correct retrieval due to dozens of seconds of stored history.

In general, decoding the physiological meaning of the spatial-temporal Ca^{2+} signaling in astrocytes, its computational properties, and its impact on neuronal signaling remains a major challenge in modern neurobiology [14]. Integration of astrocytic signaling in cognitive processing has implications for understanding the basis of cognitive dysfunction and the development of new therapeutic strategies [16]. The SNAN model proposed here could constitute a tool to investigate the role of astrocytes in cognitive functions. To facilitate a stronger link of the proposed SNAN with neuroscience, it might be interesting to employ the mechanisms of intracellular integration of Ca^{2+} signals in astrocytes [36].

Our current work and model do not consider challenges and issues related to the hardware implementation of the model. Having said this, hardware implementation of SNN models is a promising and viable modern trend in the field of neuromorphic electronics. Memristors and memristive electronics can already reproduce in silico both spiking neuron dynamics, synaptic signal transmission, and synaptic plasticity. With respect to the implementation of astrocytes and the astrocyte-to-neuron control in silico, several articles reported successful implementations of the astrocyte dynamics [22], [23], [67]. This suggests that hardware implementations of SNN-based neuromorphic memory could be viable in the near future.

Finally, we would like to comment on the biological plausibility and model limitations in capturing the behavior of real brain circuits. By construction, our neuromorphic SNN model imitates morphological constitutions of real brain networks at the macroscopic level. At this macroscopic level, the model demonstrates that involving astrocytes in the processing circuits can lead to significant improvements in memory performance, as compared to neuronal SNNs without astrocytes (see Tables S3 and S4 of the supplementary material). The proposed SNAN model reflects experimental data on the structure, connectivity, and neurophysiology of the interaction between neurons and astrocytes in the underlying cortical tissue [14], [16], [19]. As the prototype of the SNAN model, we utilize our previously published biologically plausible computational model of working memory [30]. This model consists of an SNN interacting with a network of astrocytes. In order to enhance its bio-fidelity, we enriched the model with an unsupervised synaptic learning rule based on spike-timing-dependent Hebbian plasticity, as well as a layer of inhibitory neurons [59]. Our biologically relevant, yet still general, modeling approach has ultimately provided insight into the hypothesis of astrocytes participating in memory formation. This hypothesis has emerged from various experimental findings on the contribution of astrocyte signaling to information processing and cognitive function [16], [17]. However, many of these cases lack a comprehensive understanding of the precise mechanisms underlying the astrocytic contribution, making our understanding somewhat fragmented. Therefore, further research is necessary to elucidate the specific role of astrocytic action in memory processes. It is difficult to compare true human memory with any given and fixed mathematical model as our understanding of memory and its mechanisms is far from complete. Moreover, this understanding is continuously evolving. Circuits of true memory are involved in (and are affected by) many complex biological processes, including hormonal regulations at the micro level, and emotions and stresses at the psychophysiological level. These factors may significantly affect memory performance in different "intrinsic situations," somewhat similar to what we modeled here as "external situations." In this context, by involving astrocytic components, our model offers a framework capable of accounting for factors previously considered exogenous. Remarkably, we show here that doing so is advantageous as compared to other models of memory (see Tables S3 and S4 of the supplementary material). Further steps could consider including and assessing the performance of brain circuits that are directly responsible for memory function, for example, the hippocampus. The topological organization of cells in such structures is more complicated than simple layered architectures which are typical artificial neuronal networks including SNNs. The advantage of considering more complicated topologies of networks could be to explore the existence of architectures optimizing network learning and retrieval tasks. Another point that is missed in almost all mathematical models of SNNs is structural plasticity—dynamic changes in the number of connections, neurons, and astrocytes in the network and their properties. Finally, all living networks have a differentiation facilitating

ongoing information exchange with the external world, forming processing pathways from the sensory stimuli, e.g., visual images in our case, to execution signals, and repository systems. Including, modeling, and analyzing these could be natural steps toward bringing the performance of neuromorphic SNNs to that of true living brains.

IX. Conclusion

This article presents a novel approach to temporal non-IID data organization for machine learning in spiking neuronal networks. The effectiveness of data formalization in situation-based pools is demonstrated by the short-term memory task implemented by the brain-inspired SNAN. The SNAN includes a layer of principle (pyramidal) neurons supplied by a group of inhibitory interneurons. Synaptic connections in the pyramidal layer self-adjust adaptively according to the Hebbian-like STDP. Following morphological brain synaptic organization, the pyramidal neurons are accompanied by astrocytes organized in the form of a layered network (see Fig. 3). Astrocytic modulation of neuronal activity represents the activity-dependent short-term synaptic plasticity that induces the stimulus-specific local spatial synchronization in neuronal ensembles. The synergistic interplay between fast-spiking neuronal networks trained on the general dataset and slow astrocytic syncytia provides buffering of situation-based data pools by the selective coordination of neuronal signaling, which results in successful storage and retrieval of highly overlapped information patterns. We demonstrated that the astrocyte-induced influence on synaptic transmission results in a 10% enhancement of spiking neural network memory performance in terms of correlation level between the cued retrievals and samples for strong 50% overlapped patterns.

Code Availability

The code is available at https://github.com/altergot/Neuron-astrocyte-network-Situation-associated-memory.

Acknowledgment

This study was conducted within the framework of the Scientific Program of the National Center for Physics and Mathematics, Section IX "artificial intelligence and big data in technical, industrial, natural, and social systems" [the neuromorphic memory concept development and numerical simulations (Sections IV, VI, and VII-B4 and VII-B5)] and was funded by the Russian Science Foundation [Grant 22-12-00216 for the model development (Sections V, VII-A, and VII-B1–VII-B3) and Grant 21-72-10129 for the comparative analysis (Sections VII-B6 and VII-B7 and VIII)].

References

[1] P. L. Anthony and M. Bartlett, *Neural Network Learning: Theoretical Foundations*. Cambridge, U.K.: Cambridge Univ. Press, 1999.

[2] V. N. Vapnik, "An overview of statistical learning theory," *IEEE Trans. Neural Netw.*, vol. 10, no. 5, pp. 988–999, Sep. 1999.

[3] F. Cucker and S. Smale, "On the mathematical foundations of learning," *Bull. Amer. Math. Soc.*, vol. 39, no. 1, pp. 1–49, 2002.

[4] A. Bastounis, A. C. Hansen, and V. Vlačić, "The mathematics of adversarial attacks in AI—Why deep learning is unstable despite the existence of stable neural networks," 2021, *arXiv:2109.06098*.

[5] J. Lu, A. Liu, F. Dong, F. Gu, J. Gama, and G. Zhang, "Learning under concept drift: A review," *IEEE Trans. Knowl. Data Eng.*, vol. 31, no. 12, pp. 2346–2363, Dec. 2019.

[6] I. Tyukin, A. N. Gorban, C. Calvo, J. Makarova, and V. A. Makarov, "High-dimensional brain: A tool for encoding and rapid learning of memories by single neurons," *Bull. Math. Biol.*, vol. 81, no. 11, pp. 4856–4888, Mar. 2018, doi: 10.1007/s11538-018-0415-5.

[7] A. N. Gorban, V. A. Makarov, and I. Y. Tyukin, "The unreasonable effectiveness of small neural ensembles in high-dimensional brain," *Phys. Life Rev.*, vol. 29, pp. 55–88, Jul. 2019, doi: 10.1016/j.plrev.2018.09.005.

[8] I. Y. Tyukin, A. N. Gorban, M. H. Alkhudaydi, and Q. Zhou, "Demystification of few-shot and one-shot learning," 2021, *arXiv:2104.12174*.

[9] A. N. Gorban, B. Grechuk, E. M. Mirkes, S. V. Stasenko, and I. Y. Tyukin, "High-dimensional separability for one- and few-shot learning," *Entropy*, vol. 23, no. 8, p. 1090, Aug. 2021, doi: 10.3390/e23081090.

[10] Y. Yufik and R. Malhotra, "Situational understanding in the human and the machine," *Frontiers Syst. Neurosci.*, vol. 15, Dec. 2021, Art. no. 786252, doi: 10.3389/fnsys.2021.786252.

[11] M. R. Endsley and E. S. Connors, "Foundation and challenges," in *Advances in Information Security*. Cham, Switzerland: Springer, 2014, pp. 7–27, doi: 10.1007/978-3-319-11391-3_2.

[12] A. Vaswani et al., "Attention is all you need," in *Proc. Adv. neural Inf. Process. Syst.*, vol. 30, 2017, pp. 1–15.

[13] A. Verkhratsky and M. Nedergaard, "Physiology of astroglia," *Physiolog. Rev.*, vol. 98, no. 1, pp. 239–389, Jan. 2018, doi: 10.1152/physrev.00042.2016.

[14] A. Semyanov, C. Henneberger, and A. Agarwal, "Making sense of astrocytic calcium signals—From acquisition to interpretation," *Nature Rev. Neurosci.*, vol. 21, no. 10, pp. 551–564, Sep. 2020, doi: 10.1038/s41583-020-0361-8.

[15] A. Araque, G. Carmignoto, P. G. Haydon, S. H. R. Oliet, R. Robitaille, and A. Volterra, "Gliotransmitters travel in time and space," *Neuron*, vol. 81, no. 4, pp. 728–739, Feb. 2014, doi: 10.1016/j.neuron.2014.02.007.

[16] M. Santello, N. Toni, and A. Volterra, "Astrocyte function from information processing to cognition and cognitive impairment," *Nature Neurosci.*, vol. 22, no. 2, pp. 154–166, Jan. 2019.

[17] J. Nagai et al., "Behaviorally consequential astrocytic regulation of neural circuits," *Neuron*, vol. 109, no. 4, pp. 576–596, Feb. 2021, doi: 10.1016/j.neuron.2020.12.008.

[18] P. Kofuji and A. Araque, "Astrocytes and behavior," *Annu. Rev. Neurosci.*, vol. 44, no. 1, pp. 49–67, Jul. 2021, doi: 10.1146/annurev-neuro-101920-112225.

[19] K. V. Kastanenka et al., "A roadmap to integrate astrocytes into systems neuroscience," *Glia*, vol. 68, no. 1, pp. 5–26, May 2019, doi: 10.1002/glia.23632.

[20] J. Liu et al., "Exploring self-repair in a coupled spiking astrocyte neural network," *IEEE Trans. Neural Netw. Learn. Syst.*, vol. 30, no. 3, pp. 865–875, Mar. 2019, doi: 10.1109/TNNLS.2018.2854291.

[21] S. Nazari, M. Amiri, K. Faez, and M. M. Van Hulle, "Information transmitted from bioinspired neuron–astrocyte network improves cortical spiking network's pattern recognition performance," *IEEE Trans. Neural Netw. Learn. Syst.*, vol. 31, no. 2, pp. 464–474, Feb. 2020, doi: 10.1109/TNNLS.2019.2905003.

[22] H. Soleimani, M. Bavandpour, A. Ahmadi, and D. Abbott, "Digital implementation of a biological astrocyte model and its application," *IEEE Trans. Neural Netw. Learn. Syst.*, vol. 26, no. 1, pp. 127–139, Jan. 2015, doi: 10.1109/TNNLS.2014.2311839.

[23] S. Nazari, K. Faez, M. Amiri, and E. Karami, "A digital implementation of neuron–astrocyte interaction for neuromorphic applications," *Neural Netw.*, vol. 66, pp. 79–90, Jun. 2015, doi: 10.1016/j.neunet.2015.01.005.

[24] M. Hayati, M. Nouri, S. Haghiri, and D. Abbott, "A digital realization of astrocyte and neural glial interactions," *IEEE Trans. Biomed. Circuits Syst.*, vol. 10, no. 2, pp. 518–529, Apr. 2016, doi: 10.1109/TBCAS.2015.2450837.

[25] E. V. Pankratova, A. I. Kalyakulina, S. V. Stasenko, S. Y. Gordleeva, I. A. Lazarevich, and V. B. Kazantsev, "Neuronal synchronization enhanced by neuron–astrocyte interaction," *Nonlinear Dyn.*, vol. 97, no. 1, pp. 647–662, May 2019, doi: 10.1007/s11071-019-05004-7.

[26] S. Makovkin, E. Kozinov, M. Ivanchenko, and S. Gordleeva, "Controlling synchronization of gamma oscillations by astrocytic modulation in a model hippocampal neural network," *Sci. Rep.*, vol. 12, no. 1, p. 6970, Apr. 2022, doi: 10.1038/s41598-022-10649-3.

[27] O. Kanakov, S. Gordleeva, A. Ermolaeva, S. Jalan, and A. Zaikin, "Astrocyte-induced positive integrated information in neuron–astrocyte ensembles," *Phys. Rev. E, Stat. Phys. Plasmas Fluids Relat. Interdiscip. Top.*, vol. 99, no. 1, Jan. 2019, Art. no. 012418, doi: 10.1103/physreve.99.012418.

[28] O. Kanakov, S. Gordleeva, and A. Zaikin, "Integrated information in the Spiking–Bursting stochastic model," *Entropy*, vol. 22, no. 12, p. 1334, Nov. 2020, doi: 10.3390/e22121334.

[29] L. Abrego, S. Gordleeva, O. Kanakov, M. Krivonosov, and A. Zaikin, "Estimating integrated information in bidirectional neuron-astrocyte communication," *Phys. Rev. E, Stat. Phys. Plasmas Fluids Relat. Interdiscip. Top.*, vol. 103, no. 2, Feb. 2021, Art. no. 022410, doi: 10.1103/physreve.103.022410.

[30] S. Y. Gordleeva et al., "Modeling working memory in a spiking neuron network accompanied by astrocytes," *Frontiers Cellular Neurosci.*, vol. 15, Mar. 2021, Art. no. 631485, doi: 10.3389/fncel.2021.631485.

[31] A. Zhao, A. Ermolaeva, E. Ullner, J. Kurths, S. Gordleeva, and A. Zaikin, "Noise-induced artificial intelligence," *Phys. Rev. Res.*, vol. 4, no. 4, Oct. 2022, Art. no. 043069.

[32] M. De Pittà and N. Brunel, "Multiple forms of working memory emerge from synapse–astrocyte interactions in a neuron–glia network model," *Proc. Nat. Acad. Sci. USA*, vol. 119, no. 43, Oct. 2022, Art. no. e2207912119, doi: 10.1073/pnas.2207912119.

[33] S. Becker, A. Nold, and T. Tchumatchenko, "Modulation of working memory duration by synaptic and astrocytic mechanisms," *PLOS Comput. Biol.*, vol. 18, no. 10, Oct. 2022, Art. no. e1010543, doi: 10.1371/journal.pcbi.1010543.

[34] Y. Tsybina et al., "Astrocytes mediate analogous memory in a multi-layer neuron–astrocyte network," *Neural Comput. Appl.*, vol. 34, no. 11, pp. 9147–9160, Feb. 2022, doi: 10.1007/s00521-022-06936-9.

[35] S. Y. Makovkin, I. V. Shkerin, S. Y. Gordleeva, and M. V. Ivanchenko, "Astrocyte-induced intermittent synchronization of neurons in a minimal network," *Chaos, Solitons Fractals*, vol. 138, Sep. 2020, Art. no. 109951, doi: 10.1016/j.chaos.2020.109951.

[36] S. Y. Gordleeva, A. V. Ermolaeva, I. A. Kastalskiy, and V. B. Kazantsev, "Astrocyte as spatiotemporal integrating detector of neuronal activity," *Frontiers Physiol.*, vol. 10, p. 294, Apr. 2019, doi: 10.3389/fphys.2019.00294.

[37] A. Hodgkin and A. Huxley, "A quantitative description of membrane current and its application to conduction and excitation in nerve," *Bull. Math. Biol.*, vol. 52, nos. 1–2, pp. 25–71, 1990, doi: 10.1016/s0092-8240(05)80004-7.

[38] Y. Zhang, Y. Xu, Z. Yao, and J. Ma, "A feasible neuron for estimating the magnetic field effect," *Nonlinear Dyn.*, vol. 102, no. 3, pp. 1849–1867, Oct. 2020, doi: 10.1007/s11071-020-05991-y.

[39] C. Morris and H. Lecar, "Voltage oscillations in the barnacle giant muscle fiber," *Biophys. J.*, vol. 35, no. 1, pp. 193–213, Jul. 1981, doi: 10.1016/s0006-3495(81)84782-0.

[40] Y. Xu, M. Liu, Z. Zhu, and J. Ma, "Dynamics and coherence resonance in a thermosensitive neuron driven by photocurrent*," *Chin. Phys. B*, vol. 29, no. 9, Aug. 2020, Art. no. 098704, doi: 10.1088/1674-1056/ab9dee.

[41] E. M. Izhikevich, "Simple model of spiking neurons," *IEEE Trans. Neural Netw.*, vol. 14, no. 6, pp. 1569–1572, Nov. 2003, doi: 10.1109/TNN.2003.820440.

[42] V. B. Kazantsev and S. Y. Asatryan, "Bistability induces episodic spike communication by inhibitory neurons in neuronal networks," *Phys. Rev. E, Stat. Phys. Plasmas Fluids Relat. Interdiscip. Top.*, vol. 84, no. 3, Sep. 2011, Art. no. 031913, doi: 10.1103/physreve.84.031913.

[43] P. M. Esir, S. Y. Gordleeva, A. Y. Simonov, A. N. Pisarchik, and V. B. Kazantsev, "Conduction delays can enhance formation of up and down states in spiking neuronal networks," *Phys. Rev. E, Stat. Phys. Plasmas Fluids Relat. Interdiscip. Top.*, vol. 98, no. 5, Nov. 2018, Art. no. 052401, doi: 10.1103/physreve.98.052401.

[44] M. M. Halassa, T. Fellin, H. Takano, J.-H. Dong, and P. G. Haydon, "Synaptic islands defined by the territory of a single astrocyte," *J. Neurosci.*, vol. 27, no. 24, pp. 6473–6477, Jun. 2007, doi: 10.1523/jneurosci.1419-07.2007.

[45] G. Ullah, P. Jung, and A. Cornellbell, "Anti-phase calcium oscillations in astrocytes via inositol (1, 4, 5)-trisphosphate regeneration," *Cell Calcium*, vol. 39, no. 3, pp. 197–208, Mar. 2006, doi: 10.1016/j.ceca.2005.10.009.

[46] T. Yamamoto, A. Ochalski, E. L. Hertzberg, and J. I. Nagy, "On the organization of astrocytic gap junctions in rat brain as suggested by LM and EM immunohistochemistry of connexin43 expression," *J. Comparative Neurol.*, vol. 302, no. 4, pp. 853–883, Dec. 1990, doi: 10.1002/cne.903020414.

[47] J. I. Nagy and J. E. Rash, "Connexins and gap junctions of astrocytes and oligodendrocytes in the CNS," *Brain Res. Rev.*, vol. 32, no. 1, pp. 29–44, Mar. 2000, doi: 10.1016/s0165-0173(99)00066-1.

[48] S. Y. Gordleeva, S. V. Stasenko, A. V. Semyanov, A. E. Dityatev, and V. B. Kazantsev, "Bi-directional astrocytic regulation of neuronal activity within a network," *Frontiers Comput. Neurosci.*, vol. 6, p. 92, Sep. 2012, doi: 10.3389/fncom.2012.00092.

[49] T. Fellin, O. Pascual, S. Gobbo, T. Pozzan, P. G. Haydon, and G. Carmignoto, "Neuronal synchrony mediated by astrocytic glutamate through activation of extrasynaptic NMDA receptors," *Neuron*, vol. 43, no. 5, pp. 729–743, Sep. 2004, doi: 10.1016/j.neuron.2004.08.011.

[50] N. Chen et al., "Nucleus basalis-enabled stimulus-specific plasticity in the visual cortex is mediated by astrocytes," *Proc. Nat. Acad. Sci. USA*, vol. 109, no. 41, pp. E2832–E2841, Sep. 2012, doi: 10.1073/pnas.1206557109.

[51] G. Perea and A. Araque, "Astrocytes potentiate transmitter release at single hippocampal synapses," *Science*, vol. 317, no. 5841, pp. 1083–1086, Aug. 2007, doi: 10.1126/science.1144640.

[52] M. Navarrete and A. Araque, "Endocannabinoids mediate neuron-astrocyte communication," *Neuron*, vol. 57, no. 6, pp. 883–893, Mar. 2008, doi: 10.1016/j.neuron.2008.01.029.

[53] M. Navarrete and A. Araque, "Endocannabinoids potentiate synaptic transmission through stimulation of astrocytes," *Neuron*, vol. 68, no. 1, pp. 113–126, Oct. 2010, doi: 10.1016/j.neuron.2010.08.043.

[54] A. Mazzoni, S. Panzeri, N. K. Logothetis, and N. Brunel, "Encoding of naturalistic stimuli by local field potential spectra in networks of excitatory and inhibitory neurons," *PLoS Comput. Biol.*, vol. 4, no. 12, Dec. 2008, Art. no. e1000239, doi: 10.1371/journal.pcbi.1000239.

[55] M. Chalk, P. Masset, S. Deneve, and B. Gutkin, "Sensory noise predicts divisive reshaping of receptive fields," *PLOS Comput. Biol.*, vol. 13, no. 6, Jun. 2017, Art. no. e1005582, doi: 10.1371/journal.pcbi.1005582.

[56] S. A. Lobov, M. O. Zhuravlev, V. A. Makarov, and V. B. Kazantsev, "Noise enhanced signaling in STDP driven spiking-neuron network," *Math. Model. Natural Phenomena*, vol. 12, no. 4, pp. 109–124, 2017, doi: 10.1051/mmnp/201712409.

[57] H. Noh, T. You, J. Mun, and B. Han, "Regularizing deep neural networks by noise: Its interpretation and optimization," in *Proc. Adv. Neural Inf. Process. Syst.*, vol. 30, 2017, pp. 1–13.

[58] I. A. Surazhevsky et al., "Noise-assisted persistence and recovery of memory state in a memristive spiking neuromorphic network," *Chaos, Solitons Fractals*, vol. 146, May 2021, Art. no. 110890, doi: 10.1016/j.chaos.2021.110890.

[59] K. Roy, A. Jaiswal, and P. Panda, "Towards spike-based machine intelligence with neuromorphic computing," *Nature*, vol. 575, no. 7784, pp. 607–617, Nov. 2019, doi: 10.1038/s41586-019-1677-2.

[60] J. C. R. Whittington, J. Warren, and T. E. J. Behrens, "Relating transformers to models and neural representations of the hippocampal formation," 2021, *arXiv:2112.04035*.

[61] V. A. Demin et al., "Necessary conditions for STDP-based pattern recognition learning in a memristive spiking neural network," *Neural Netw.*, vol. 134, pp. 64–75, Feb. 2021, doi: 10.1016/j.neunet.2020.11.005.

[62] Z. Wang et al., "Fully memristive neural networks for pattern classification with unsupervised learning," *Nature Electron.*, vol. 1, no. 2, pp. 137–145, Feb. 2018, doi: 10.1038/s41928-018-0023-2.

[63] D. Querlioz, O. Bichler, P. Dollfus, and C. Gamrat, "Immunity to device variations in a spiking neural network with memristive nanodevices," *IEEE Trans. Nanotechnol.*, vol. 12, no. 3, pp. 288–295, May 2013, doi: 10.1109/TNANO.2013.2250995.

[64] V. Matrosov, S. Gordleeva, N. Boldyreva, E. Ben-Jacob, V. Kazantsev, and M. D. Pittà, "Emergence of regular and complex calcium oscillations by inositol 1, 4, 5-trisphosphate signaling in astrocytes," in *Computational Glioscience* (Springer Series in Computational Neuroscience). Cham, Switzerland: Springer, 2019, pp. 151–176, doi: 10.1007/978-3-030-00817-8_6.

[65] M. Lukoševičius and H. Jaeger, "Reservoir computing approaches to recurrent neural network training," *Comput. Sci. Rev.*, vol. 3, no. 3, pp. 127–149, Aug. 2009, doi: 10.1016/j.cosrev.2009.03.005.

[66] P. R. Vlachas et al., "Backpropagation algorithms and reservoir computing in recurrent neural networks for the forecasting of complex spatiotemporal dynamics," *Neural Netw.*, vol. 126, pp. 191–217, Jun. 2020, doi: 10.1016/j.neunet.2020.02.016.

[67] F. Azad, M. Shalchian, and M. Amiri, "Circuit modelling of 2-AG indirect pathway via astrocyte as a catalyst for synaptic self repair," *Anal. Integr. Circuits Signal Process.*, vol. 95, no. 1, pp. 127–139, Jan. 2018, doi: 10.1007/s10470-018-1106-8.

Susanna Gordleeva received the M.Sc. and Ph.D. degrees in physics and mathematics from the Lobachevsky State University of Nizhny Novgorod, Nizhny Novgorod, Russia, in 2010 and 2015, respectively, and the D.Sc. (Habilitation) degree in biophysics from the Institute of Theoretical and Experimental Biophysics RAS, Pushchino, Russia. in 2022.

Since 2015, she has been serving as an Assistant Professor in computational neuroscience at Lobachevsky State University, Nizhny Novgorod. In 2021, she became the Head of the Laboratory of Neurodynamics and Cognitive Technologies, Institute of Neuroscience, Lobachevsky State University. In 2022, she was appointed as a Professor in computational neuroscience. She is currently a Professor at the Department of Neurotechnologies, Lobachevsky State University. Her research interests encompass theoretical neuroscience, computational neurobiology, neurotechnology, and mathematical biology.

Yuliya A. Tsybina received the B.Sc. and M.Sc. degrees in radiophysics from the Lobachevsky State University of Nizhny Novgorod, Nizhny Novgorod, Russia, in 2017 and 2019, respectively.

She is currently a Junior Researcher with the Lobachevsky State University of Nizhny Novgorod, and Sechenov First State Medical University, Moscow, Russia. Her research interests include nonlinear dynamics of neuronal systems, spiking neural networks, neuron-astrocyte interaction, and models of synaptic plasticity and learning.

Mikhail I. Krivonosov received the B.Sc. and M.Sc. degrees in applied mathematics and computer science from the Lobachevsky State University of Nizhny Novgorod, Nizhny Novgorod, Russia, in 2016 and 2018, respectively.

He is currently a Junior Researcher with the Lobachevsky State University of Nizhny Novgorod. His research interests include image processing, explainable AI, and complex networks.

Ivan Y. Tyukin received the M.Sc., Ph.D., and D.Sc. (Habilitation) degrees from Saint Petersburg Electrotechnical University, Saint Petersburg, Russia, in 1998, 2001, and 2006, respectively.

After the Ph.D. degree, he worked as a Research Scientist at RIKEN Brain Science Institute, Wako, Japan. Since then, he became a Lecturer in applied mathematics, a Reader, and a Professor in applied mathematics in 2012, 2014, and 2018, respectively. From 2019 to 2021, he was an Adjunct Professor at the Norwegian University of Science and Technology (NTNU), Trondheim, Norway. In 2022, he moved to King's College London, London, U.K., where he is currently a Professor of mathematical data science and modeling at the Department of Mathematics. His research interests span mathematical modeling, control, optimization, data analysis, and mathematical foundations of AI and machine learning.

Dr. Tyukin was awarded an RCUK Academic Fellowship at the University of Leicester, Leicester, U.K., in 2007. In 2021, he was awarded a UKRI Turing AI Acceleration Fellowship to work on the mathematics underpinning the development of robust, stable, and resilient AI. He is an Editorial Board Member of *Industrial Artificial Intelligence* and *Computational Mathematics and Modeling* and an Editor of *Communications in Nonlinear Science and Numerical Simulation*.

Victor B. Kazantsev is a Professor and the Head of the Department of Neurotechnologies, Institute of Biology and Biomedicine, Lobachevsky State University of Nizhny Novgorod, Nizhny Novgorod, Russia. He previously founded and served as the Head of the Department of Neurodynamics and Neurobiology, Faculty of Biology, Lobachevsky State University of Nizhny Novgorod, in 2005, which has since been renamed to the Department of Neurotechnologies, Institute of Neurochemistry, UNN. From 2015 to 2020, he was the Vice-Rector for Research at the Lobachevsky State University of Nizhny Novgorod. He has authored more than 200 scientific publications. His prominent scientific accomplishments include the development of a neuromorphic control system for multiparametric objects, which simulates the dynamics of neurons in the inferior olives of the brain, ensuring the maintenance of motor patterns with a large number of dynamic variables in real-time. He has participated in the development of a multimodal human–machine interface that transmits signals from human muscles and the brain to control external information devices, including exoskeletons, wheelchairs, and automobiles (neuromobile). His interests include theoretical neuroscience, computational neurobiology, neurotechnology, and mathematical biology.

Alexey Zaikin has a Chair of systems medicine and applied mathematics at UCL, London, U.K., sharing this appointment between the Department of Mathematics and the Institute for Women's Health. He has published over 160 articles on topics in interdisciplinary fields, including systems biology and medicine, stochastic processes, nonlinear dynamics, data analysis, statistics, and artificial intelligence. These works developed new statistical methodologies for the early diagnosis of cancer, including algorithms for detecting network oncobiomarkers, new parameter estimation methods, Bayesian methods for detecting change points for longitudinal oncobiomarkers, new methods for analyzing trends in serial oncobiomarkers, and the methodology of synolitic network analysis based on graphs. His research interests included an investigation of intelligence and consciousness. These papers have also shown that the presence of astrocytes: 1) improves the generation of integrated information, meaning that the development of astrocytes was necessary for the emergence of consciousness; 2) is responsible for a short-term memory formation in a model of interacting neural and astrocytic networks at times of increasing intracellular calcium concentration in astrocytes due to astrocytic modulation of synaptic transmission; and 3) is important for new biophysical models of glia-mediated processes in the brain associated with pattern recognition, aging and neurodegenerative diseases.

Alexander N. Gorban has been a Personal Chair in applied mathematics at the University of Leicester, Leicester, U.K., since 2004. He worked for Russian Academy of Sciences, Siberian Branch, Krasnoyarsk, Russia, and ETH Zürich, Zürich, Switzerland, was a Visiting Professor and a Scholar at Clay Mathematics Institute, Cambridge, MA, USA, IHES, Bures-sur-Yvette, France, Courant Institute, New York City, NY, USA, and Isaac Newton Institute for Mathematical Sciences, Cambridge, U.K. Now, he is the Director of the Centre for Artificial Intelligence, Data Analysis and Modeling (AIDAM), University of Leicester, and the Principal Research Fellow with King's College London, London, U.K. His main research interests are machine learning, data mining and model reduction problems, kinetics, and applied dynamics. His main results (obtained with coauthors) include the solution to Hilbert's sixth problem, algorithms and theory of error correction for AI systems in a high-dimensional world, mechanisms of working memory in neural-astrocytic networks, methods of topological grammars for exploratory data analysis and methods of invariant manifold for chemical and physical kinetics. He predicted dynamics of correlation graphs between various features of the organism during stress and adaptation and developed methods of early anticipation of critical transitions used for many systems. In dynamics, he developed the detailed theory of slow transition processes and critical retardation with applications in chemistry and physics.